ELSEVIER

International Journal of Minerals, Metallurgy and Materials
Volume 16, Number 3, June 2009, Page 265

Metallurgy

Effect of sinter layer porosity distribution on flow and temperature fields in a sinter cooler

Jik-chang Leong[1)], *Kai-wun Jin*[1)], *Jia-shyan Shiau*[2)], *Tzer-ming Jeng*[3)], *and Chang-hsien Tai*[1)]

1) Department of Vehicle Engineering, Pingtung University of Science and Technology, China Taipei

2) Iron Making Process Development Section, Steel & Aluminum Research & Development Department, China Taipei

3) Department of Mechanical Engineering, Air Force Institute of Technology, China Taipei

(Received 2008-05-26)

Abstract: When sinters are filled into the sinter cooler from the sintering machine, it is commonly seen that, due to segregation effects, sinters of larger size usually accumulate closer to the inner wall of the sinter cooler, whereas those of smaller size are to the outer wall. This nonuniform distribution of sinters has led to uneven cooling effect throughout the cooler. This causes the sinters leaving the cooler at a large temperature difference. This undesired temperature difference leads to the deformation and even the destruction of the conveyors. The computational fluid dynamics (CFD) technique was used in the present work to investigate the heat and fluid flow phenomena within the sinter cooler corresponding to the different distribution of sinter layer porosity, which was highly dependent on the arrangement and orientation of sinters within the sinter cooler. It is confirmed that a high mass flow rate within the sinter layer causes a low temperature region and *vice versa*. The flow fields for vertically reducing porosity distribution and random distribution are almost identical indicating the relative insignificance of convective heat transfer mechanism.

Key words: steel plant; sinter cooler; sinter; porosity; heat transfer; packed bed

1. Introduction

Fire ore, lump ore of size less than 10 mm, and other fluxes are mixed evenly to form the raw materials of sinter with right composition before they are sent to the sintering machine. At the sintering machine, extremely hot sinter bed is formed. The sinter bed is then crashed into smaller pieces by a breaker before it is fed into the sinter cooler from the distributor. As the sinter cooler rotates, hot sinters are gradually cooled down before they are sent to the bin of blast furnace stock house *via* a series of conveyors.

In the upper trays of the sinter cooler, the sinters are expected to cool down. To further enhance the cooling effect, an air passage is constructed directly beneath the trays. As air is blown into the passage from the fans, pressure is built up within the air passage and therefore air is forced to percolate the sinter layer. When the cool air flows around the sinters and leaves the sinter cooler from top, it brings the thermal energy away from the sinters. The effectiveness of the sinter cooler actually greatly depends on the porosity of the sinter layer. When sinters fall from the distributor, segregation effect is bounded to occur. Because of the difference in size, sinters of greater size are more likely to roll further, whereas the smaller ones are closer to the distributor. This causes an uneven distribution of sinter size in the cooler. Therefore, air prefers to flow through the sinter layer where its local porosity is great. In short, uneven sinter size distribution will eventually result in uneven heat removal and relatively low cooler efficiency.

Zhao *et al.* [1] analyzed the sinter organizational structure associated with the No.3 sintering machine trolley section of the Shuicheng Iron and Steel Corporation using optics microscope and X-ray diffraction. Although their work was not directly related to a sinter cooler, they pointed out a phenomenon observed related to a sinter cooler. Before entering the sintering machine, the raw materials are fed into the trolley from a fixed location. In the trolley, the raw materials form a hill-shape pile at the location where most raw materials land. Under the influence of gravitational force, materials of larger size tend to automatically

Corresponding author: Chang-hsien Tai, **E-mail:** chtai@mail.npust.edu.tw

Also available online at www.sciencedirect.com

roll off the pile and scatter around the edge of the pile. As the trolley is moving, this segregation effect is more clearly seen in the transverse direction of the trolley causing the materials coarser in average at both the trolley side walls and finer at the trolley center. As a result, the permeability of the raw material mixture becomes highly nonuniform, the flow nearby the trolley side walls is greater and therefore the cooling is faster close to side walls.

In another work, Chang *et al.* [2] investigated the influences of air velocity from an air-flow feeding device and water contents in raw materials on the segregation effects. They found that there existed a suitable range of air velocity within which segregation effect was enhanced with air velocity. If the air velocity was too low, the materials were generally unaffected; if the velocity was too large, the materials were blown away leading to excessive loss. In their study, the optimum air velocity produced the best segregation effect.

More recently, Zhang *et al.* [3] discovered that it was possible to characterize the sinter size distribution with different MgO contents by fractal dimension. This fractal dimension was a linear function of MgO content and was also an excellent quantitative indication of sinter distribution, spread phenomenon and homogeneity, as well as the crack degree of sinters.

In a recent non-published work, BlueScope Steel Co. used screen method to separate the sinters into several classes of different sizes. Evenly, the coarsest sinters are laid at the base of the sinter cooler, whereas the finest were laid at the uppermost. With this orientation, cool air could homogeneously percolate the sinter layers and therefore effectively cooled down the sinters.

Zhu *et al.* [4] have successfully established a mathematical model describing the temperature distribution of rolling billets from the heater, roller, and water box. Their model was a combination of a two-dimensional modeling of the first-two rollers with a one-dimensional model for rest of the rollers. Based on their model, the main thermal characters of a rolling line could be simulated. The parameters in their model included the billet material, its discharge temperature, and dimension (*i.e.* width and height). Their results were comparable to the field data with a relative error of 2%.

The size distribution of the sinters in the sinter cooler is random. The modeling of the hydrodynamics of a packed bed is commonly accomplished through a few models satisfying basic physical principles, as well as involving several experimentally determined parameters. More than half a century ago, Ergun [5] had proposed a correlation for the pressure drop across a random packed bed. The two parameters appeared in his well-known correlation depend on conditions such as the geometry of the grains filling the packed bed, the voidage of the bed, and the wall roughness. Calis *et al.* [6] examined the feasibility of using commercially available CFD software to predict the pressure drop corresponding to a single-phase flow penetrating a packed bed. Their results obtained from CFX-5.3 coincided relatively well with experimental data with an average error of only approximately 10% if the tube-to-particle diameter ratio was between 1.0 and 2.0. Not only so, the velocity field obtained through numerical means was comparable with those obtained using Laser-Doppler Anemometry. More importantly, they had verified that the k-ε turbulence model could adequately simulate packed bed of spheres.

Andrade *et al.* [7] computationally investigated the origin of the deviation from the classical Darcy's Law by simulating two-dimensional disordered porous media. For different porosities and flow conditions, they applied Forchheimer formulation to estimate the friction factor. Also, based on experimental observations, they found that the importance of flow inertial effect increases with Reynolds number starting from linearly to nonlinearly mainly because of the characteristics of kinetic energy distribution within the interstitial pore space. Moreover, the transition from linearity to nonlinearity takes place in the range of $10^{-2}<Re'<10^{-1}$, where Re' is defined as $Re'=\beta\rho KV/\mu$. Here, β is the inertial parameter in the Forchheimer formulation, ρ the fluid density, K the permeability of the porous structure, V the velocity, and μ the fluid viscosity.

The objective of this work was to numerically investigate the sinter temperature field in the cooler for different distributions of sinter porosity. By recognizing the interrelationship between the porosity distribution and the temperature field, the design of the sinter distributor and sinter cooler of a steel company could be improved or redesigned. This work used GAMBIT and FLUENT to perform the simulation of relevant flow and temperature fields. To better approximate the behaviors of the sinter filled in the cooler, the principles of porous media were employed. A typical sinter cooler is schematically shown in Fig. 1. Sinters are fed into the cooler from a distributor. Although the cooler rotates in the counter-clockwise direction, the sinters are slowly being cooled by the air blown into the air passage through the fans. This cooling process takes about 40 min and ends by the transferring of sinters from the cooler to the conveyors.

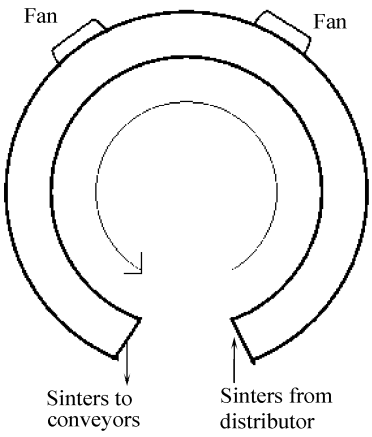

Fig. 1. Configuration of the sinter cooler studied in this work.

2. Methods

2.1. Computational model

This study combined the control volume finite-difference technique, the SIMPLE approach [8], the concept of moving reference frames, the standard k-ε turbulence model [9], and the Brinkman-Darcy-Ergun porous model [10] to simulate the flow and temperature fields within the entire sinter cooler. Several assumptions were made in this study to simplify the model: air was incompressible in this case because its corresponding Mach number was sufficiently less than 0.3; the flow field was quasi-steady and therefore its turbulence phenomena could be modeled using the k-ε turbulence model; the behavior of the sinter layer was assumed to be suitably approximated using a packed bed of spheres; and thermal loss to the surrounding through radiation could be neglected.

CFD approach was used to solve the following three-dimensional steady-state governing equations for primarily the velocity, pressure, and temperature fields simultaneously.

Continuity equation:

$$\frac{\partial u_i}{\partial x_i} = 0 \tag{1}$$

Navier-Stokes equation:

in the air passage,

$$\frac{\partial}{\partial x_i}\left(u_i u_j\right) = -\frac{1}{\rho}\frac{\partial p}{\partial x_j} + \frac{1}{\rho}\frac{\partial \tau_{ij}}{\partial x_i} \tag{2}$$

in the sinter layer,

$$\frac{\partial}{\partial x_i}\left(u_i u_j\right) = -\frac{1}{\rho}\frac{\partial p}{\partial x_j} + \frac{1}{\rho}\frac{\partial \tau_{ij}}{\partial x_i} + \frac{\mu_e}{\rho}\frac{\partial^2 u_i}{\partial x_i^2} + \frac{S_j}{\rho} \tag{3}$$

Among various turbulence models, this work uses the standard k-ε turbulence model for its ease of use. The governing equations are shown below.

k equation:

$$\frac{\partial}{\partial x_i}\left(k\overline{u_i}\right) = \frac{1}{\rho}\frac{\partial}{\partial x_i}\left[\left(\mu + \frac{\mu_t}{\sigma_k}\right)\frac{\partial k}{\partial x_i}\right] + \frac{G_k}{\rho} - \varepsilon + \frac{S_k}{\rho} \tag{4}$$

ε equation:

$$\frac{\partial}{\partial x_i}\left(\varepsilon\overline{u_i}\right) = \frac{1}{\rho}\frac{\partial}{\partial x_i}\left[\left(\mu + \frac{\mu_t}{\sigma_\varepsilon}\right)\frac{\partial \varepsilon}{\partial x_i}\right] + \frac{C_{1\varepsilon}}{\rho}\frac{\varepsilon}{k}\left(G_k\right) - C_{2\varepsilon}\frac{\varepsilon^2}{k} + \frac{S_\varepsilon}{\rho} \tag{5}$$

The terms appeared in Eqs. (4)-(5) are defined as:

$$\mu_t = \rho C_\mu \frac{k^2}{\varepsilon} \tag{6}$$

$$G_k = \mu_t S_s^2 \tag{7}$$

$$S_s = \sqrt{2S_{ij}S_{ij}} \tag{8}$$

$$S_{ij} = \frac{1}{2}\left(\frac{\partial \overline{u_i}}{\partial x_j} + \frac{\partial \overline{u_j}}{\partial x_i}\right) \tag{9}$$

where x_i is the coordinate system in the i-direction; u_i the air velocity component in the x_i direction; P the pressure; τ_{ij} the stress tensor; ρ the density; μ_e the fluid effective dynamic viscosity; S_j the additional term in the j-porous media momentum equation; μ the fluid dynamic viscosity; S_k the turbulence kinetic energy source term; G_k the production of turbulence kinetic energy; S_ε the dissipation of turbulent kinetic energy source term. The constants involved in Eqs. (4)-(6) are σ_ε=1.30, σ_k=1.00, $C_{1\varepsilon}$=1.44, $C_{2\varepsilon}$=1.92, and C_μ=0.09. Since the classical Darcy's law is only accurate for very low speed flow in low porosity porous media, Forchheimer accounted for flows in porous matrix with a greater velocity and hence improved the classical Darcy's law by introducing a new term that takes the inertia of the fluid into consideration. This additional term considers the form drag and surface drag that the fluid experiences as it flow through the porous media. On the other hand, Brinkman suggested that the nonslip velocity condition must not be violated for a bounded porous media. Therefore, the pressure drop in a porous media must obey Brinkman-Darcy-Ergun formulation [5]. The additional term S_j in Eq. (3) is expressed as follows where the inertial coefficient F is estimated through the well-known Ergun correlation. This model is shown below:

$$S_j = \frac{\partial p}{\partial x_j} = -\frac{\mu}{\alpha}u_j - \frac{F\rho}{\sqrt{\alpha}}\left|u_j\right|u_j \tag{10}$$

$$\alpha = \frac{\gamma^3 d_p^2}{150(1-\gamma)^2} \tag{11}$$

$$\mu_e = \mu \tag{12}$$

$$F = \frac{1.75}{\sqrt{150}\gamma^{1.5}} \tag{13}$$

where γ is the porosity, d_p the particle diameter, and μ_e the fluid effective dynamic viscosity, which Brinkman assumed simply equivalent to the fluid dynamic viscosity μ.

To solve the temperature distribution in the entire sinter cooler, the following energy equations are solved separately for the sinter cooler and its air passage.

In the air passage:

$$\frac{\partial Eu_i}{\partial x_i} = \frac{1}{\rho}\frac{\partial}{\partial x_i}\left(k_f \frac{\partial T}{\partial x_i}\right) \tag{14}$$

In the sinter cooler:

$$\frac{\partial Eu_r}{\partial x_i} = \frac{1}{\rho}\frac{\partial}{\partial x_i}\left(k_{eff} \frac{\partial T}{\partial x_i}\right) \tag{15}$$

In Eq. (15), the angular velocity of air in the sinter cooler is given as $u_r = \omega \cdot r$, where ω is the rotational speed of the sinter cooler, and r the radial distance from the axis of rotation. Since the sinter layer is spatially occupied by both sinters and air surrounding them, it is essential to introduce an effective thermal conductivity k_{eff} for the sinter layer. Shonnard and Whitaker [11] had proposed a mean of estimating k_{eff} based on the thermal conductivities of the solid (*i.e.*, the sinter) and the fluid (*i.e.*, the air). The correlation is given as

$$k_{eff} = k_f\left[4\ln(k_s/k_f) - 11\right] \tag{16}$$

where k_f and k_s are the thermal conductivities of the fluid phase (including the turbulence thermal conductivity) and solid phase, respectively.

2.2. Computational domain and conditions

The computational domain in this work consisted of the sinter layer with the air passage beneath it. Fig. 2(a) shows the sinter layer (upper) and the air passage (lower). The sinter layer has a uniform height of *H,* while the height of the air passage varies. The distribution of the structured grid constructed using Gambit is shown in Fig. 2(b).

In this simulation, sinters were assumed entering the sinter cooler at a temperature of 800 K, whereas air entered at a gage pressure and temperature of 100 Pa and 300 K, respectively. The air left the sinter cooler at a gage pressure of 0 Pa. The sinter cooler rotated very slowly at a rotational speed of 0.0025 rad/s. All solid walls were assumed insulated and satisfy no-slip boundary condition. Furthermore, the properties of the sinters were assumed similar to those of iron, *i.e.*, its density was 7897 kg/m^3, its heat capacity was 452 J/(kg·K)$^{-1}$, and its thermal conductivity was 73 W/(m·K)$^{-1}$.

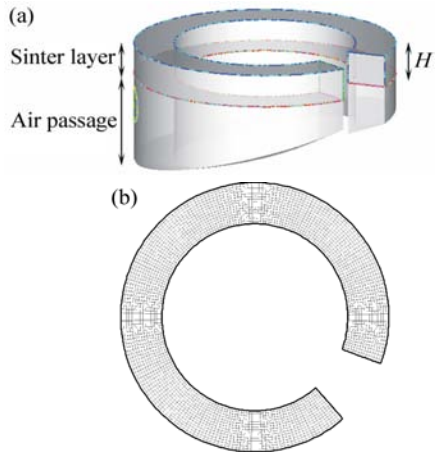

Fig. 2. Geometry of the sinter cooler and its air passage: (a) isometric view; (b) top view.

In order to customize the distribution of sinter layer porosity, a C program (also referred to User-Define-Functions) was added into the FLUENT solver to define the variations of porosity and particle diameter as functions of radial location and height. Also, the fact that sinters at high temperature entered the sinter cooler continuously was approximated by defining a prescribed heat flux at the inter inlet surface.

3. Results and discussion

3.1. Flow pattern in the air passage

The air passage beneath the sinter cooler ($-20° \le \theta \le 313°$, $-2.7 \le z/H \le 0.0$, $2.8 \le r/H \le 4.0$) and the two fans installed to blow cooler air into the air passage have been shown in Fig. 1. The parameter z indicates the vertical coordinate of the system starting from the bottom of the sinter cooler. Fig. 3 show the pressure and vertical velocity distributions at $z/H = -0.4$. Since the fans blow cool air into the air passage at 300 K, the pressure is the highest on the inner wall across the fan inlets where the air may become stagnant. According to Fig. 3(a), the velocity magnitude is apparently the greatest at the locations closest to the fan inlets, and the air stream is diverted to flow azimuthally and vertically as it gets closer to the inner wall where the local pressure is high (Fig. 3(b)). Although air flow at this height is vertically upward, the vertical velocity magnitude is mainly greater than 0.2 m/s. Furthermore, it is re-

markable to see that the vertical velocity at the regions next to the outer wall between the fans and the sinter inlet or outlet is generally higher than other places.

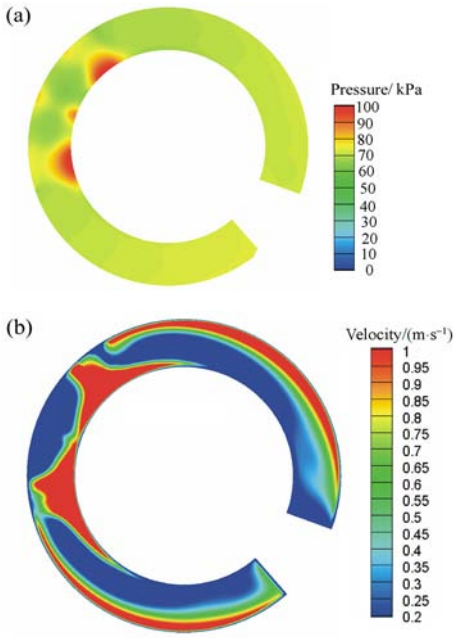

Fig. 3. Distributions of vertical velocity (a) and pressure (b) at z/H=–0.4.

3.2. Radially reducing porosity distribution

If the sinters are arranged that its porosity varies linearly from 0.5 at the inner sinter cooler wall to 0.3 at the outer sinter cooler wall, it means the sinters are larger in size at the inner wall than the outer wall. Fig. 4 shows the distribution of vertical velocity at z/H=0.2. It is clear that more air flow through the sinter layer where porosity is large. However, it is seen that the distribution of vertical velocity is slightly disturbed close to the fan outlets and the inner wall sections across them. The kinetic energy introduced by fans has provided the air with more inertia to overcome greater flow resistance due to smaller porosity and is therefore capable of penetrating the sinter layer at a greater r/H ratio.

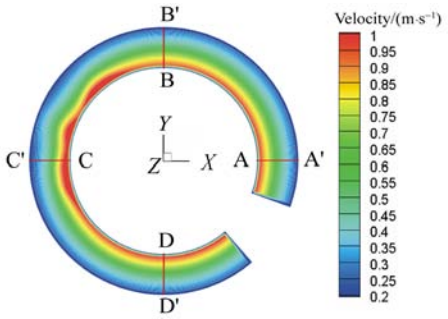

Fig. 4. Velocity distributions for radially reducing sinter layer porosity.

Fig. 5 display the distributions of vertical velocity vectors at cross-sections A-A', B-B', C-C', and D-D' shown in Fig. 4. The edges A', B', C', and D' represent the outer wall. The height z/H = 0.0 represents the interface between the sinter layer (upper) and the air passage (lower). Obviously, the velocity vectors in the sinter layer are longer near the inner wall (edges A, B, C, and D) and are shorter near the outer wall (A', B', C', and D'). This implies that most air penetrates the sinter layer where porosity is greater, whereas there is almost no flow next to the outer wall where porosity is the lowest. Section C-C' shows that at the location close to the fan outlets, air impinges the inner wall (edge C) causing a local high pressure region. This pushes the air into the sinter layer. Also, the presence of a strong vortex can be clearly seen at the lower region transporting the kinetic energy from the inner wall region to the outer wall region. For this reason, air in the air passage at cross-sections A-A', B-B', and D-D' tends to flow upward along the outer wall under the influence of the aforementioned vortex. Fig. 6 depicts the velocity and temperature distributions on the surface where sinters leave the sinter cooler. The greatest mass flow rate takes place on the inner wall and at the same time, the temperature at the outer upper corner remains significantly as high as 797 K. The lowest temperature takes place at the inner lower corner. This is because the low porosity at the outer wall leads to high flow resistance and eventually suppresses the mass flow rate that in turn effectively reduces the temperature of the sinters over there.

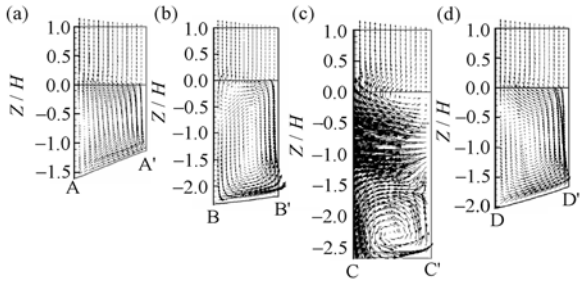

Fig. 5. Distributions of vertical velocity vectors at different cross-sections in Fig. 4: (a) A-A'; (b) B-B'; (c) C-C'; (d) D-D'.

3.3. Vertically reducing porosity distribution

If the sinters are arranged such that its porosity varies linearly from 0.5 at the sinter layer base to 0.3 at the sinter layer surface, it means smaller sinters are placed on the top of the larger ones. Fig. 7 shows the distribution of vertical velocity at z/H=0.2. In this case, the sinter porosity only depends on elevation (z/H). In general, the vertical velocity is almost uniform everywhere except at the regions close to the fan outlets where the air is forced to change direction. As shown in Fig. 8, the air velocity in the sinter layer is the smallest as it enters the sinter layer and becomes the

greatest as it leaves the layer. This phenomenon satisfies the principle of mass conservation because the effective void area is greater at the sinter layer base. Since the sinter porosity is merely a function of elevation, air leaving the sinter upper surface nearly has the same velocity. Within the air passage, the air flow pattern is almost identical to those shown in Fig. 5. If compared carefully, it can be observed that air in the air passage at sections A-A' and D-D' shown in Fig. 5 tends to enter the sinter layer close to the inner wall where the flow resistance is the least. In this case, the porosity at the interface between the sinter layer and the air passage is the same. Air in the air passage has no incentive to flow toward the inner wall before entering the sinter layer.

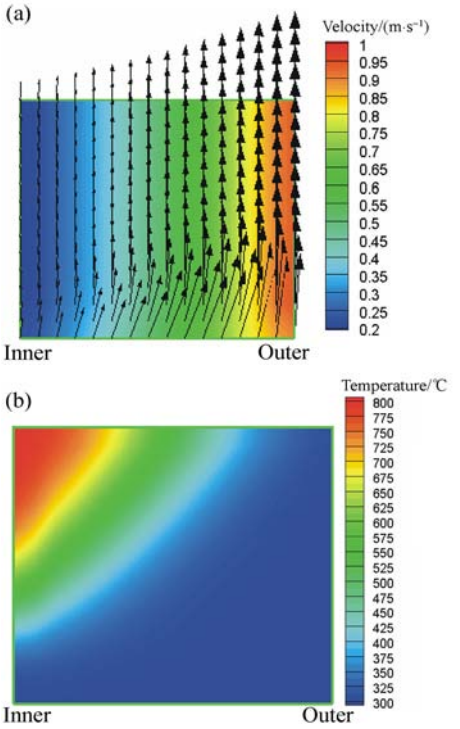

Fig. 6. Velocity vector (a) and temperature profile (b) at the sinter outlet surface for radially reducing sinter layer porosity.

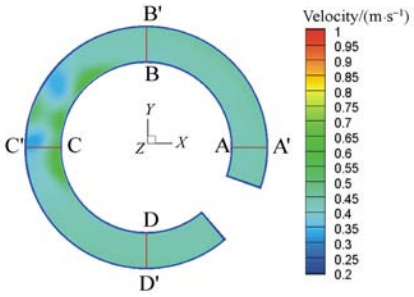

Fig. 7. Velocity distributions for vertically reducing sinter layer porosity.

Fig. 9 shows the velocity and temperature distributions on the surface where sinters leave the cooler. Since the sinter layer porosity is uniform in the radial direction but decreases linearly with elevation, the length of the velocity vectors not only indicates that air enters the sinter layer at a greater velocity than it leaves the uppermost surface but also it leaves at the same velocity. The temperature distribution, on the other hand, proves that the temperature is generally stratified implying the absence of significant local convective effect. In this case, the highest temperature is 716 K.

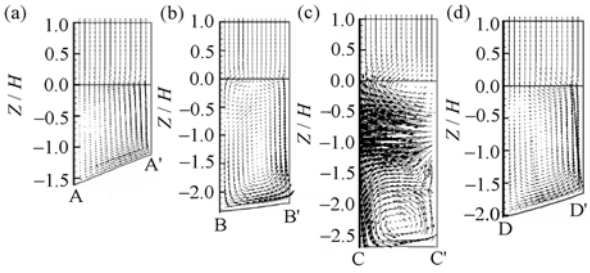

Fig. 8. Distributions of vertical velocity vectors at different cross-sections in Fig. 7: (a) A-A'; (b) B-B'; (c) C-C'; (d) D-D'.

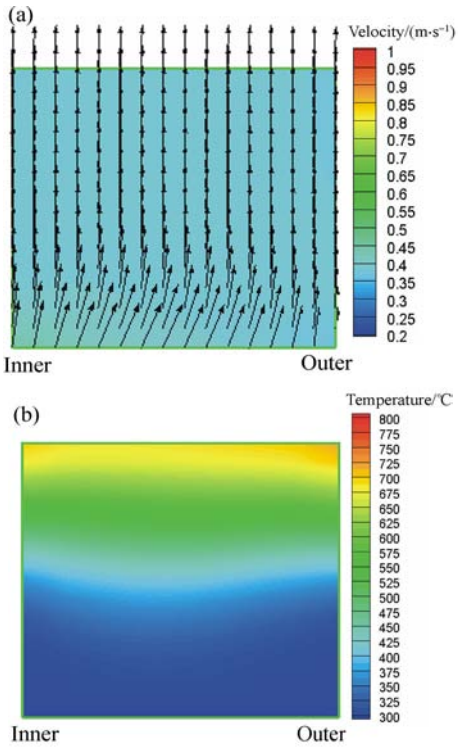

Fig. 9. Velocity vector (a) and temperature profile (b) at the sinter outlet surface for vertically reducing sinter layer porosity.

3.4. Outward reducing porosity distribution

The flow and temperature fields shown in Figs. 10-12 correspond to a sinter layer whose porosity equals to 0.5 at the center and linearly decreases to 0.3 at the two edges. This physically means that the size of sinters is the greatest at the center and the smallest at the inner and outer walls. Fig. 10 shows the distribution of vertical velocity at z/H=0.2. With this poros-

ity distribution, the vertical velocity is the greatest at the center and reduces almost linearly in both radial directions. At the regions close to the fan outlets, the additional pressure produced by the fans further increases the local vertical velocity. Fig. 11 further demonstrates the velocity profile proving that the mass flow rate decreases linearly from the center to the walls. Similar to Fig. 5, the flow patterns in the air passage are almost the same. Since the flow resistance of the sinter layer is the lowest at the center, most of the air in the air passage gathers at the center and then enters the sinter layer. Only when the flow inertia is significantly close to the fan outlets, the air after impinging the inner is less likely to make a sharp turn in the passage before entering the sinter layer. The flow field depicted in Fig. 12(a) has further proven the fact that the lower sinter layer porosity at the center leads to lower flow resistance and therefore greater velocity. Although the temperature distribution in this case (Fig. 12(b)) is very much different from those discussed previously, it is apparently a combination of that shown in Fig. 6(b) with a symmetrical reflection. Even so, the maximum temperature found in this surface is 791 K.

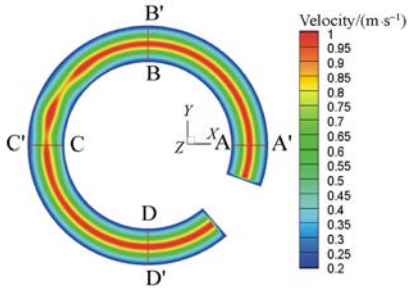

Fig. 10. Velocity distributions for outward reducing sinter layer porosity.

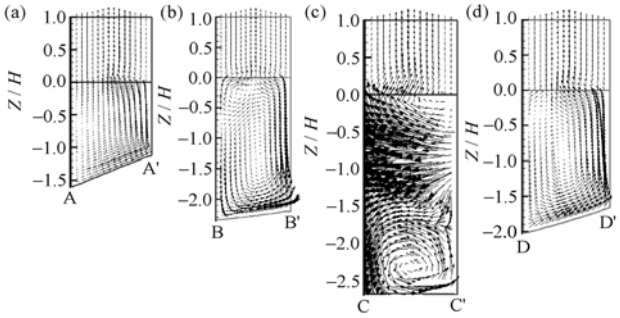

Fig. 11. Distributions of vertical velocity vectors at different cross-sections in Fig. 10: (a) A-A'; (b) B-B'; (c) C-C'; (d) D-D'.

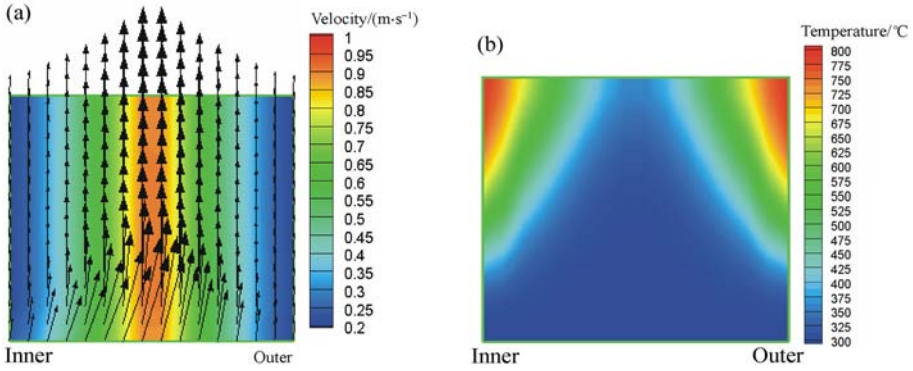

Fig. 12. Velocity vector (a) and temperature profile (b) at the sinter outlet surface for outward reducing sinter layer porosity.

3.5. Random porosity distribution

In reality, it is rather difficult to completely control the porosity of the sinter layer as it is highly dependent on the segregation process when the sinter cooler is filled up. As a comparison, a random distribution of porosity is investigated. The distribution of vertical velocity at z/H = 0.2 is illustrated in Fig. 13, and the distributions of vertical velocity vectors at cross-sections A-A', B-B', C-C', and D-D' shown in Fig. 13 are displayed in Fig. 14.

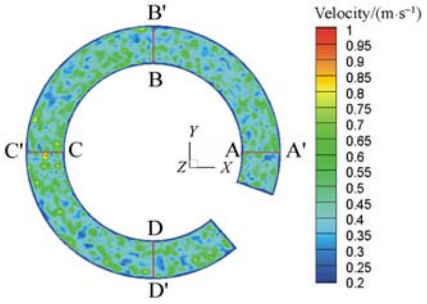

Fig. 13. Velocity distributions for random sinter layer porosity.

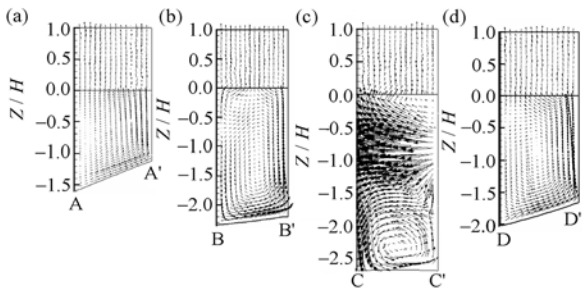

Fig. 14. Distributions of vertical velocity vectors at different cross-sections in Fig. 13: (a) A-A'; (b) B-B'; (c) C-C'; (d) D-D'.

With porosity distribution being randomized, the maximum magnitude of the vertical velocity reduces to roughly 0.6 m/s. However, it is remarkable to find that the placement of fan has very insignificant effect on the vertical velocity distribution. Because of the random porosity, the flow in the sinter layer does not follow any particular pattern in terms of direction and magnitude. Even so, both the sinter layer with random porosity distribution and that whose porosity decreases linearly upward have a similar effect on the air pattern in the air passage. On the surface where sinters leave the sinter cooler, the flow in the sinter layer is obviously random in nature, as seen in Fig. 15(a). Despite the disorder nature of velocity field, its corresponding temperature field shows a high degree of resemblance with that in Fig. 9(b). This also suggests that the local convective effect is negligible. The highest temperature on this surface is now 689 K, which is lower than that of vertically reducing porosity distribution.

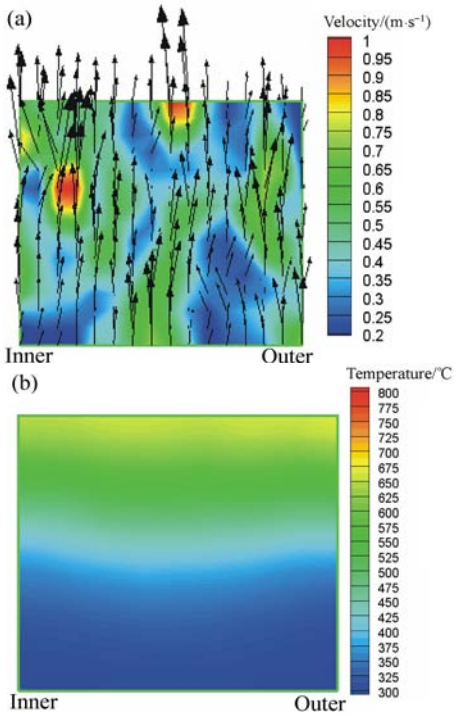

Fig. 15. Velocity vector (a) and temperature profile (b) at the sinter outlet surface for random sinter layer porosity.

4. Conclusions

A series of simulations have been successfully performed to investigate the flow and temperature fields in a sinter cooler and its air passage. The effect of sinter layer porosity has been studied by considering 4 types of porosity distribution. Several conclusions can be achieved as follows.

(1) If the sinter layer porosity varies in the radial direction, there always exists at least a ring of region associated with a high mass flow rate. This high mass flow rate causes a low temperature region, at the same time, a low mass flow rate region where the temperature is high.

(2) Although the flow patterns are very dissimilar if the sinter layer porosity varies vertically or randomly, the temperature distributions in them are very similar. This suggests that the convective effect in both these porosity distributions is insignificant.

(3) The air flow pattern in the air passage is almost independent on the porosity distribution within the sinter layer. The very thin layer beneath the sinter layer is the only noticeable region.

References

[1] Y.P. Zhao, H.L. Deng, J.G. Xiao, W.Z. Ao, and J.Z. Zhang, The sinter organizational structure analyses of the 3# sintering machine trolley section in Shuigang, *J. Guizhou Univ. Technol.* (in Chinese), 35(2006), No.3, p.18.

[2] L.L. Chang, B. Xu, and T. Jiang, Research of Air-flow Feeding in Sinter, *Min. Metall. Eng.* (in Chinese), 27(2007), No.2, p.54.

[3] Y.Z. Zhang, Y. Xu, X.G. Si, Q.J. Zhang, and X.G. Ma, Research on size distribution of sinters with different MgO content, *Iron Steel* (in Chinese), 42(2007), No.9, p.12.

[4] H. Zhu, X. Hao, W. Zhi, Y. Zhang, and H. Chen, Mathematical model for the thermal process of controlled cooling of wires and its numerical simulation, *J. Univ.Sci. Technol. Beijing*, 11(2004), No.6, p.505.

[5] S. Ergun, Fluid Flow through Packed Columns, *Chem. Eng. Prog.*, 48(1952), No.2, p.89.

[6] H.P.A. Calis, J. Nijenhuis, B.C. Paikert, F.M. Dautzenberg, and C.M. van den Bleek, CFD modelling and experimental validation of pressure drop and flow profile in a novel structured catalytic reactor packing, *Chem. Eng. Sci.*, 56(2001), p.1713.

[7] J.S. Andrade Jr., U.M.S. Costa, M.P. Almeida, H.A. Makse, and H.E. Stanley, Inertial effects on fluid flow through disordered porous media, *Phys. Rev. Lett.*, 82(1999), No.26, p.5249.

[8] S.V. Patankar, *Numerical Heat Transfer and Fluid Flow*, Hemisphere Publishing Corporation, New York, 1980.

[9] B.E. Launder and D.B. Spalding, *Lectures in Mathematical Models of Turbulence*, Academic Press, London, 1972.

[10] M. Kaviany, *Principle of Heat Transfer in Porous Media*, Springer-Verlag New YorkInc., 2nd Ed., New York, 1995, p.52.

[11] D.R. Shonnard and S. Whitaker, The effective thermal conductivity for point contact porous medium: an experimental study, *Int. J. Heat Mass Transfer*, 32(1989), p.503.